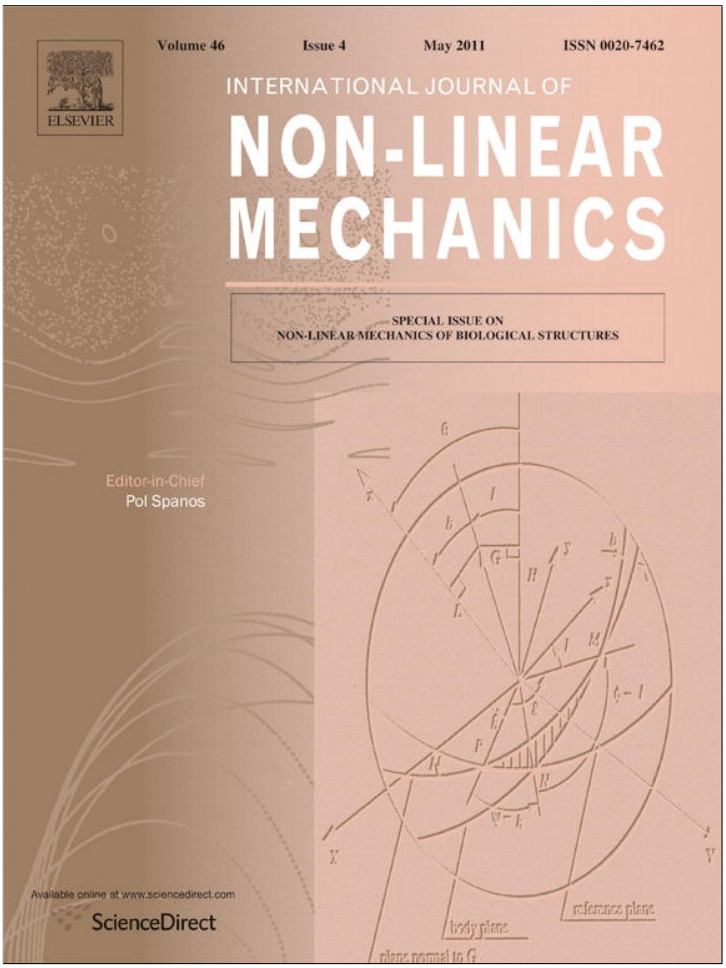

International Journal of Non-Linear Mechanics 46 (2011) 616–626

Contents lists available at ScienceDirect

International Journal of Non-Linear Mechanics

journal homepage: www.elsevier.com/locate/nlm

A theory for the hydrodynamic origin of whale flukeprints

R. Levy [a,*], D. Uminsky [b], A. Park [a], J. Calambokidis [c]

[a] Department of Mathematics, Harvey Mudd College, 301 Platt Blvd., Claremont, CA 91711, USA
[b] Department of Mathematics, UCLA 7619C Mathematical Sciences, 520 Portola Plaza Box 951555, Los Angeles, CA 90095-1555, USA
[c] Cascadia Research, 218 1/2W 4th Ave., Olympia, WA 98501, USA

ARTICLE INFO

Available online 23 December 2010

Keywords:
Whale
Flukeprint
Footprint
Vortex ring
Vortex shedding
Wave damping
Breakwater
Surfactant

ABSTRACT

Whale flukeprints are an often observed, but poorly understood, phenomenon. Used by whale researchers to locate whales, flukeprints refer to a strikingly smooth oval-shaped water patch which forms behind a swimming or diving whale on the surface of the ocean and persists up to several minutes. In this paper we provide a description of hydrodynamic theory and related experiments explaining the creation and evolution of these "whale footprints." The theory explains that the motion of the fluke provides a mechanism for shedding of vortex rings which subsequently creates a breakwater that damps the short wavelength capillary waves. The theory also suggests that the role of natural surfactants are of secondary importance in the early formation of these prints.

1. Introduction

Flukeprints are a visible pattern that appears on the surface of the ocean when a whale is swimming at a shallow depth or beginning a terminal dive. Whale-watchers can easily observe these striking oval-shaped prints on the surface of the ocean. The outer edge of the print is accentuated by small ridges, where wave-breaking may occur. The interior of the print is smooth compared to the surface outside the print, since very few capillary (wind-driven) waves are visible as in Fig. 1. The print grows radially and may remain visible for as long as several minutes, depending on ocean and wind conditions. A popular name for this phenomenon is "whale footprint" since the prints can be used to track whales over long distances as they migrate. While smaller swimming animals such as dolphins and manatees create surface prints, whales create the largest prints with the longest duration.

There is no extensive research on the phenomenon of whale prints. A study conducted concurrently with this one uses aerial photographs to determine that the water temperature in the prints is lower than that of the surrounding water, indicating that the water in the print has been brought from below the surface [1]. At the same time, the glossy, slick-like appearance of the print and the fluid ridge at its edge is reminiscent of small oil slicks. This has fueled popular theories that surfactants (surface tension-reducing substances) create the prints [2–4]. In the case of slicks made by surfactants, gradients in surfactant concentration (changes in the concentration of surfactant on the surface of a liquid) cause a surface stress. The surface is pulled to regions of higher tension, and small disturbances are stretched out. This "calming of the waters" by surfactants such as oil or soap has been observed since ancient times [5]. In addition, the calm water in the far wake of navy sea ships has been shown to have lower surface tension than water outside the wake, which has been attributed to natural ocean surfactants brought to the surface in the wake [6–8]. Other literature attributes hydrodynamic forces, such as vortices, as the origin of flukeprints [9,10].

Marine biologists note that there are several reasons that surfactants might be present in flukeprints. One hypothesis concerns the whale's oily skin, which could act as a surfactant. Whales shed their oily skin at approximately 50 times the rate of humans [11]. The skin is usually exfoliated during social activities such as lobtailing and breaching [12], and skin fragments can subsequently be found near the whale's flukeprints. Although researchers collect skin samples from flukeprints, the material is sparse and not always evident. Therefore, the volume of skin sloughed may be too small to cause a significant surfactant effect. Another possibility is that algae, remains of feeding and other particulate matter brought to the surface may act as surfactants [13]. While any of these effects could be present to enhance the formation or duration of the flukeprint, we will argue below that the evidence is not compelling as the primary origin of the prints.

To summarize, two primary mechanisms have been proposed for the formation of flukeprints, a general "upwelling" of water off the fluke and a surfactant-based explanation. In this paper we propose that the dominant mechanism is the motion of the water induced by the movement of the fluke. We will demonstrate that in order to understand flukeprints, new fluid mechanics are not required. However, several aspects of existing theory must be

* Corresponding author. Tel.: +1 909 607 6019; fax: +1 909 621 8366.
E-mail addresses: levy@math.hmc.edu (R. Levy), duminsky@math.ucla.edu (D. Uminsky), allison_park@hmc.edu (A. Park), calambokidis@cascadiaresearch.org (J. Calambokidis).

0020-7462/$ - see front matter © 2011 Elsevier Ltd. All rights reserved.
doi:10.1016/j.ijnonlinmec.2010.12.009

Fig. 1. Typical flukeprint from humpback whale (*Megaptera novaeangliae*). Inside the print, the surface is smooth due to a lack of short capillary waves. Long wavelengths persist. At the boundary, wave-breaking has occurred. (Photo courtesy of Kuanyin Moi.)

combined to provide an accurate perspective on this interesting phenomenon. The characteristics of the flukeprints will be explained as a result of the hydrodynamic shedding of powerful vortex rings off the edge of the whale's fluke during swimming/diving and the ring's subsequent interaction with the ocean's surface and waves.

2. Oceanographic evidence

Our theory will be based on observations of real flukeprints made by whales, hydrodynamic theory in the literature, and experiments with a robotic fluke. We begin with observations of real flukeprints by marine biologists at Cascadia Research. The researchers film blue, humpback and gray whales above and underwater at close range by approaching the whales in small boats. The observations provide strong evidence that hydrodynamics are the primary mechanism for print formation.

The first observation is that prints are created during two different phases of swimming behavior. One occurs when whales are swimming horizontally below the surface. Whales swimming this way for a distance can be tracked by the prints, which occur at fairly regular intervals with each beat of the fluke [1]. The other time prints appear is when a whale begins a deep dive. Such "terminal dives" take place after the whale has surfaced for air and (especially in the case of humpback whales) after the characteristic sighting of the near-vertical fluke as the whale dives. These prints tend to be larger and result from strong thrusts of the fluke at the beginning of a dive.

The second observation is that a buoyant object (such as an orange) thrown into a flukeprint consistently moves to the outer edge of the print. This indicates that there is steady movement of water from the center of the print to the edge. Since this movement occurs at a range of times in which the print is visible and not just during the formation of the print, the motion is unlikely to be caused by a gradient in surfactant concentration, which would die out as the concentration rapidly equilibrates.

The third observation is one made by divers filming whales underwater. They observed vortices being shed from a blue whale fluke as the whale began a terminal dive. The motion indicated strong hydrodynamic forces originating below the surface when the whale was fluking.

The fourth observation, captured in Fig. 1, is wave breaking at the boundary of the smooth area which remains throughout the visible duration of the flukeprint. This wave phenomenon is an important consequence of the induced surface current created by the fluke hydrodynamics and will be discussed in the next section.

A fifth observation, notable in the photograph of Fig. 1, is that while small wavelength capillary waves (small surface ripples) are absent in the print, long wavelength waves are still evident. This is typical of whale flukeprints observed in the ocean. This has been experimentally observed by Evans [14] in the context of pneumatic breakwaters, discussed in Section 3.

In addition to the five observations made by the researchers at Cascadia, a sixth observation is made in an article presenting work concurrent with this research, in which flukeprints of a female humpback are observed in infrared aerial photographs originally intended to locate fish in Alaska [1]. The prints are visible in the infrared images because the temperature of the water in the prints is less than that of the ocean surface temperature outside the prints. The researchers model the difference in temperature between the nearby sea surface temperature and the temperature at the center of the prints. Using a simple hydrodynamic model in which a jet of water the width of the fluke mixes turbulently with the surface water, the cooling of the water in the print is described using an exponential function. The measurable difference in surface temperatures inside and outside the flukeprint support the theory that the prints are created as the motion of the flukes brings water to the surface of the ocean, but does not address the role of vorticity or surfactants in the formation of the prints. The cooling is attributed to turbulent mixing, and the simple model primarily exhibits exponential cooling over time. Our theory will be consistent with this observation of temperature difference between interior and exterior surface water, but will also address the formation and characteristic look of the prints.

The six observations regarding whales in natural habitats confirm that fluke motion brings water to the surface and induces an outward surface current. The remainder of this paper will be dedicated to explaining the non-linear hydrodynamics of print formation based on our theory that prints are formed by vortex ring shedding and subsequent interaction of the ring with the free surface. In other words, we will explain the phenomenon of whale footprints as a process, starting at the fluke and ending with a smooth surface. This process occurs in roughly three stages: swimming and vortex shedding, ring and surface interactions, and finally, ring-induced surface current and dampening of short waves. We will develop a coherent theory which draws upon many aspects of mathematical biology and engineering literature, including numerical simulations, mathematical models, and laboratory experiments.

3. Damped and lengthened gravity waves

As mentioned above, the most striking feature of the flukeprint is the smooth patch on the surface of the ocean, where the short capillary waves have been damped out. This localized dampening of shorter wavelengths is explained by the hydrodynamic theory of pneumatic breakwaters. A pneumatic breakwater is a jet of fluid directed at the surface, created from below by air bubbles. The bubbles entrain fluid that move to the surface and then outward. The strong horizontal (or radial) outward surface current disrupts oncoming waves, motivating the name breakwater. Early theory and experiments describing the effect of a pneumatic breakwater can be found in two papers from the 1955 Proceedings of the Royal Society A. In these companion papers, Taylor and Evans [14,15] discuss an experiment in which bubbles released from the bottom

of a tank create an upwelling of current which disrupts surface waves.

In these experiments, surface waves were generated to mimic wind-driven capillary waves that might be found in a ship harbor. The rising jet of fluid brought to the surface by the bubbles creates a surface current which is proposed as a mechanism to disrupt oncoming ocean waves. We now briefly review this theory. One of the main questions that Taylor [15] attempted to answer is: How fast must a current of a given depth, h, flow in order that it may disrupt all waves of length λ_0 or shorter?

First let us define a wave of length $\lambda = 2\pi/k$ to have frequency $\sigma/2\pi$ and let U be the uniform velocity of the current over a finite depth h. Enforcing continuity of the fluid and balancing the pressure Taylor derives the following dispersion equation:

$$\frac{(1-Y)^2(1-\alpha Y)}{(1-Y)^4-\alpha Y} = -\tanh\left(\frac{ZY}{\alpha}\right), \tag{1}$$

where Y, Z, and α are the non-dimensional variables defined as

$$Y = \frac{kU}{\sigma}, \quad \alpha = \frac{g}{U\sigma}, \quad Z = \frac{hg}{U^2}, \tag{2}$$

and g is the gravitational constant.

In the wave stopping regime, in which current is directed against oncoming waves, $U<0$ and hence the sign of α and Y are both negative. Remarkably, from Eq. (1), for a fixed Z, Y may take on any value in $(-\infty,0)$ but $-\alpha$ always has a minimum value $-\alpha_m$ which falls in the range of (0,4). In the context of flukeprints, we assume the water is deep. Thus a wave with frequency $\sigma/2\pi$ has wavelength $\lambda = 2\pi g/\sigma^2$ and by the definition of α, Taylor concludes that all waves of length less than

$$\lambda_0 = \frac{2\pi(U\alpha_m)^2}{g}$$

cannot propagate against a current of velocity U with depth h. For example, to stop a wave with a wavelength of 100 ft (a very long wave) Taylor calculates that one would need an opposing velocity of 45 ft/s with a depth of 0.34 ft or 15 ft/s at a depth of 1.6 ft, both of which represent a tremendous amount of power. On the other hand, if one wants to stop all waves of 2 ft or less (still much longer than a wind-driven capillary wave) one only needs to generate a uniform current of $U=-1$ ft/s at depth of 0.1 ft, which is well within the ability of a humpback whale at cruising speeds [1]. It is also clear from the dispersion relation (1) that while waves can be disrupted by a horizontal current initiated by a vertical jet of fluid, for reasonable current velocities only the shorter wavelengths are easily eradicated.

Unfortunately, since only long wavelengths were of concern in the ship harbors, the mechanism was not deemed viable for the protection of ships. Nevertheless, Taylor's theory, confirmed by Evan's experiments provide us with an explanation of why long wavelength patterns are visible in flukeprints, while smaller wavelengths are disrupted. The fluid sent to the ocean surface by the fluke, once at the surface, travels radially outward from the center of the print, creating an effect analogous to the currents Taylor and Evans produced with a jet of fluid or with a stream of bubbles. The outward current then disrupts the shorter wavelength wind-driven capillary waves, leaving a visibly smooth region containing only long wavelength oscillations such as those in the photograph of Fig. 1.

The key feature to this wave stopping phenomena is the wave interaction with an opposing current. Taylor provides a simple theory as to why there are no short wavelengths on the interior of a flukeprint but one feature that is not directly explained is the wave-breaking that is observed on the outer part of the ring. Wave breaking normally occurs when a wave is amplified to unstable heights and eventually crests and breaks. To explain this feature one needs to consider the theory of wave amplification by Longuet-Higgins and Stewart [16]. In [16] the authors use a careful energy argument to show that for a wave with a fixed length λ, the amplitude of this wave is given by

$$\alpha \propto [c(c+2U)]^{-1/2},$$

where $c=\sqrt{g/k}$ is the group velocity of the wave. Thus as $U\to -\frac{1}{2}c$ the amplitude, $\alpha\to\infty$. Of course, in reality the wave will break much earlier than this, but the theory provides the mechanism as to why there is a region of wave-breaking.

Brevik [17] combines the work of Taylor and Evans, as well as the theory of Longuet-Higgins and Stewart, to classify the phenomena of wave interaction with opposing currents into three distinct regions. Region I is characterized by wave amplification in which "oncoming waves meet the current and become shortened as the current becomes stronger." In addition, "…short waves increase in amplitude more rapidly than long waves." Region II is marked by wave-breaking which is wavelength dependent (shorter waves break more easily). Region III is marked by the maximum velocity of the current where rapid wave dampening occurs. A schematic of the three regions can be seen in Fig. 2. He then compares this deep water theory to large scale pneumatic breakwater experiments conducted at a finite depth, D. Brevik notes that the theory shows reasonable agreement when λ is approximately the same order as D. It is also observed that "…for the shortest wavelengths it is easier to damp the waves than the foregoing theory predicts…" which he attributes to turbulent dissipation absorbing a larger fraction of the wave energy.

The three regions are a convenient classification, motivated by experimental observation, and depend on the assumption that the induced wave current is gradual. In our case, the fluid jet created by a whale is powerful and the induced surface current is not gradual. In this case, Brevik predicts a shrinking of Region I or in some cases a collapsing of Regions I and II into a single zone where rapid amplification and breaking occurs for short wavelengths and then, behind that, a calm Region III where short waves have been damped out. This theory explains the observed wave breaking at the edge of the fluke print as seen in Fig. 1. Finally, Region III is the damped or partially damped region seen as the smooth part inside the flukeprint. From Taylor's wave stopping theory we know that inside Region III the short waves are damped out first. From observation the long wavelengths that persist inside whale flukeprints are on order of the radius of the flukeprint. Returning to Taylor's calculations outlined above, an induced current of 1 ft/s at a depth of 0.1 ft is all that is needed to stop waves of length 2 ft.

To summarize, pneumatic breakwater experiments and theory are consistent with oceanographic observations of flukeprints, provided that fluke motion can create a pneumatic jet effect on the surface. In the next few sections, we will explain how flukeprints seen on the ocean surface are a direct consequence of a vortex ring shed from the fluke. Vorticity is created during the downstroke on the underside of the fluke and then shed on the upstroke toward the surface. As it drifts toward the surface, this vortex ring creates a powerful jet of fluid that is circulated from

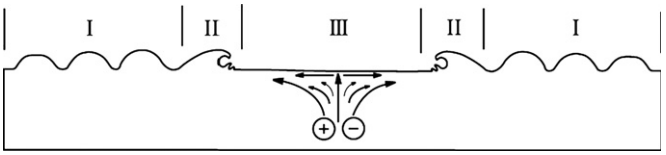

Fig. 2. A schematic drawing of the three regions corresponding to those described by Brevik in [17] and applied to a wave packet interacting with an opposing, radially outward current. Region I represents the region just outside of the flukeprint. Region II is the edge of the flukeprint, where wave-breaking occurs. Region III is the smooth interior of a flukeprint.

below the ring, through the center and then out of the top of the ring. In addition to the damping of short waves, this jet creates the long-lasting and dramatic temperature gradients on the ocean surface found in flukeprints (as shown in [1]) by bringing colder water from below the ring to the surface efficiently and in large quantities.

4. Swimming and vortex shedding

The fluid dynamics of swimming has been heavily studied in the mathematics, engineering and biology literature. While the main focus of this body of research is often the study of thrust, muscle mechanics, and efficiency, the dynamics of the vorticity shed in the wake of a swimmer has also been examined quite extensively, see [18–24]. In two dimensions, fluke motion (in water) or a flapping wing (in air) sheds a dipole pair (a two-dimensional analog of a vortex ring) in the downstream wake of the flow. The dipole pair is ejected at an angle related to the final angle of the up and down stroke and the shape of the fluke/wing, see [20,23]. The idealized non-linear dynamics of the repeated and rapid motion creates what is known as a reverse von Karman street (a sequence of dipole pairs) in the swimmer's wake.

While dipoles provide some insight and qualitative understanding of the wake of the whale in swimming, to explain a flukeprint we will need a three-dimensional non-linear theory and more evidence from actual swimming bodies. In the context of dolphins and humans, Mittal et al. [21,22] use detailed three-dimensional simulations which demonstrate numerically the shedding of vortex rings during swimming and the associated fluid jet created by the rings. In these simulations, vortex rings are shed on the up and down strokes of a dolphin's fluke or of a human's legs performing a dolphin kick (swimming on one's back underwater with legs together and kicking). On the upstroke for both the dolphin and human simulation, the ring travels upward and then dissipates. In related work, Dong et al. (2006) simulate fluid dynamics created by pectoral fins using an immersed boundary method to provide three-dimensional simulations of the vortex topology in the wake of a thin ellipsoidal flapping foil. Their simulations show that the primary topology for the vorticity consists of "two sets of interconnected vortex loops that evolve into distinct vortex rings as they convect downstream." More recently Borazjani and Sotiropoulos [18] demonstrate numerically, the shedding of vortex ring-like structures by simulating not just a detached fluke but the entire carangiform shape during swimming.

Precise measurement and analysis of vortex ring shedding in the context of fish swimming was done by Lauder and collaborators [25–27]. Lauder et al. were able to carefully record and measure the full three-dimensional velocity fields using digital particle image velocimetry (DPIV) in the wake of sunfish and sun perch and clearly demonstrate the three-dimensional vortex ring shedding off the back of the pectoral fin. Moreover, a relationship of body angle to vortex ring ejection angle was demonstrated showing a three-dimensional analog of the reverse von Karman street associated with improved thrust and more efficient swimming locomotion.

Since it is clear that vortex ring structures are indeed produced during swimming, it is important to understand how these rings interact with the ocean surface. In the next section we discuss ring-surface collisions and show how the angle of approach to the free surface affects the formation of the flukeprint.

5. Vortex ring collisions with a free surface

To better understand how flukeprints are formed during cruising and diving, we must understand the highly non-linear interaction between a vortex ring and a free surface. Theoretical, numerical, and experimental methods have been used extensively to study vortex ring collisions with a free surface. The literature categorizes collision into two regimes: head-on collisions, see [28–31], and oblique collisions [32–34]. In this body of work, the researchers generate well-controlled vortex rings using a pulse of fluid from a nozzle or, in the case of the numerical methods, assume an idealized torus shape rather than directly generating a vortex ring using a fluke. While vortex rings shed from whale flukes are imperfect and generally more turbulent, these idealized and repeatable experiments (or simulations) provide an excellent quantitative and qualitative description of surface interactions.

We note here that the associated Reynolds number (Re) for swimming whales, computed with the swim speed and the fluke length, falls into the range of Re $10^4 - 10^6$. Most of the experimental and numerical literature cited above fall in the range of Re $10^1 - 10^4$. Practically speaking, as the Reynolds number increases so does the complexity and turbulent behavior of the fluid which can create computational difficulties. Fortunately, even though the Reynolds numbers found in the literature are smaller than those realistic for whales, the observed collision dynamics in flukeprints share common features characteristic of head-on and oblique collisions. We begin by describing the main features of the dynamics of head-on collisions.

For our theory of flukeprint formation, the most important feature of head-on collision dynamics is that a jet of fluid hits the surface and immediately creates a strong radially symmetric outward current on the part of the surface directly above the ring. Outside this area, the induced radial velocity drops off rapidly as the radial surface current is circulated underneath the surface. This strong radial surface velocity will persist while the core of the ring approaches the surface, deforms and moves radially outward itself. Depending on the Reynolds number and other factors, eventually the originally coherent ring will begin to break up and slow its outward movement. During this break up, secondary and surface normal vorticity will develop and attach to the surface. A schematic illustrating the early dynamics of a head-on collision can be found in Fig. 3.

In the case of oblique collision, the non-linear dynamics are significantly more complex than the head-on case. Oblique collisions are highly three-dimensional, sensitive to the angle of

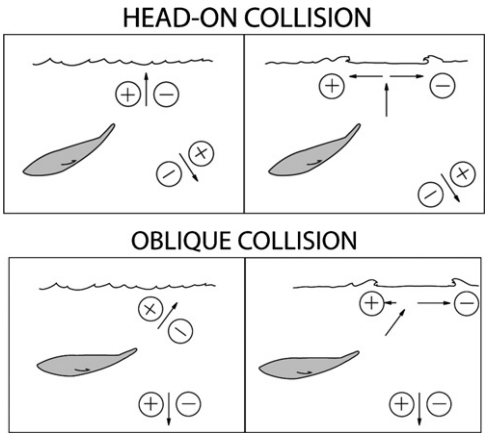

Fig. 3. Head-on collision (top): A two-dimensional schematic diagram of the early ejection of a head-on vortex ring (top left) followed by a schematic of the surface interaction (top right). The fluke is up and angled at about 60° from horizontal. Notice the symmetry of the collision allows for balanced radial outward movement of the ring during surface interaction. Oblique collision (bottom): A two-dimensional schematic diagram of the early ejection of an oblique ring (bottom left) followed by a schematic of the surface interaction (bottom right). The fluke is up and angled at about 12.5° from horizontal. Notice the leading edge of the vortex ring drifts only slightly to the left while the trailing edge spreads rapidly to the right.

collision, and thus cause the onset of three-dimensional instabilities to appear earlier in the dynamics. The early fluid motion before impact with the surface is very similar to that of a head-on collision. As described by Ohring and Lugt [32], "The fluid motion through the hole of the vortex torus resembles a round jet with a central axis, which is directed against the free surface with a stagnation point…." An excellent numerically simulated example of the localized, radially outward surface current can be seen in Fig. 5 of [32]. Next, when the leading (upper) edge of the ring becomes too close to the surface, the dynamics rapidly depart from the head-on collision case. Instead of the ring spreading symmetrically outward, a striking heart-shaped surface signature is created. This shape is captured in shadowgraph experiments in the work of both Gharib and Weigand [33], and Song et al. [34], see Fig. 4. Note that the early-time development of the heart shape occurs as the vortex ring interacts with the surface in both the uncontaminated (surfactant free) and contaminated (surfactant present) cases.

The phenomenon is caused by the leading edge of the ring colliding and attaching to the surface while the trailing edge continues to propagate. Soon after the leading edge attachment, three-dimensional instabilities begin to dominate the dynamics, the heart-shaped ring begins to break up, and surface normal vorticity develops. While the induced surface velocity field in the early dynamics creates the necessary strong radially outward current due to the vortex ring, the actual "footprint" of this current will generally be smaller due to the earlier break up of the vortex ring.

To summarize, the main early feature of both the head-on and oblique surface collisions is the creation of a strong radially outward pointing surface current induced by the vortex ring jet. In the head-on collision case the induced surface current remains roughly radially symmetric and the print grows in time. Three-dimensional instabilities and surface vorticity develop which can be seen as small surface eddies. In the oblique case, the jet induces a radially outward current followed soon afterward by the characteristic heart-shaped surface signature. Soon after the appearance of this signature, fully three-dimensional instabilities cause more significant surface normal vorticity to develop which would also be observable as surface eddies. In the next section we show in laboratory experiments that in both regimes, a fluke can create many of the same early subsurface and surface fluid dynamics as the idealized vortex rings described here.

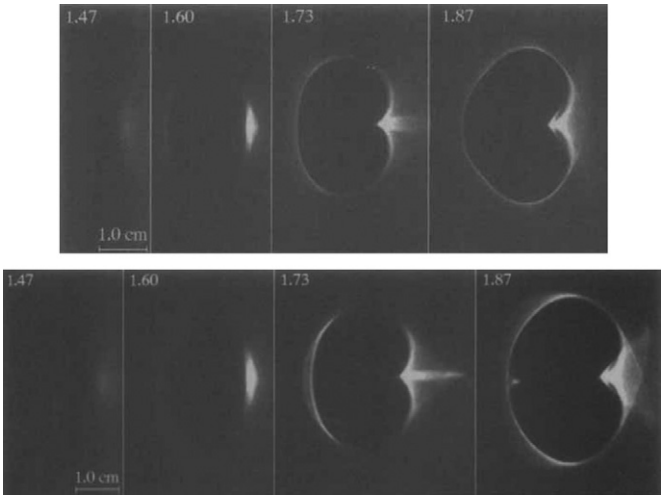

Fig. 4. Shadowgraph of vortex–surface interaction for oblique collision of vortex ring with flow from left to right at angle of 7° from horizontal for (top) uncontaminated and (bottom) contaminated surface. (Images reprinted from Figs. 3a and b, pp. 64–65 of [33] with permission from *J. Fluid Mech.*) Heart-shaped surface pattern occurs at early times with or without the presence of surfactants (contaminants).

6. On the role of naturally occurring ocean surfactants in the formation of flukeprints

Thus far, we have explained all of the primary characteristics of flukeprints. Damped interior short wavelengths, persisting interior long wavelengths, and edge wave-breaking can all be explained through the interactions of a vortex ring with the ocean surface. In this section, we will describe why surfactants might play a secondary role, enhancing the visibility and duration of the prints.

Damping of short waves in the wake of a sea body has been well studied in the context of ships [6–8]. Two smooth bands of water are commonly observed near each edge of the wake where short surface waves (≤ 20 cm wavelength) are significantly damped. This phenomenon can extend for many miles behind the ship. It has been shown by Milgram et al. [7] and Peltzer et al. [6] that these bands contain high concentrations of surfactants. The surfactants were observed using a spreading oil technique to make careful measurements in ship wakes. The spreading oil method indicated a surface tension drop of over 15% in the outer bands of the wake, compared to the surface tension outside of the wake. The precipitous drop is associated with the presence of surfactants which would lower the surface tension in these bands. Using radar images, they were also able to successfully correlate this region of high surfactant concentration to a significant lowering of the energy of short waves (≤ 20 cm wavelength), i.e. a dampening of short waves.

It is argued that the mechanism which concentrates these "natural" ocean surfactants has roughly four stages. The first is the creation of white water and bubbles generated by breaking bow, stern, and shoulder waves and the propeller wake flow. The bubbles are efficient natural surfactant harvesters since surfactants are attracted to the air–liquid interface of the bubbles. The bubbles rise to the surface, pop and deposit surfactant at the air–water interface. The surfactants are driven horizontally outward to the edge of the wake by currents generated when a vortex pair is shed off the back of the ship.

Independent of the presence of surfactant, it is worth noting that the surface velocities generated from the vortex pair shed in the wake of a ship and their effect on surface waves have been studied numerically. Using perturbation methods, [35] and direct numerical simulation [36], numerical studies aim to explain the wave behavior in the wake of ships. It should also be noted that a vortex pair generates an upward jet of fluid very similar to both a pneumatic breakwater and a vortex ring. The authors of [35,36] do not draw upon the breakwater and wave/current interaction theory we describe in Section 3, yet their simulations exhibit behavior consistent with this theory. Specifically, the simulations show that the surface current that results from a trailing vortex pair near the surface of the ocean will shift energy from waves moving across the wake from higher to lower frequencies, causing a dampening of the short waves. This happens in the region directly above the vortex pair which has the effect of allowing only long wavelengths to persist in this region while not allowing shorter wavelengths. Using real ship wake measurements, the authors in [35] show that the simulations of damped short waves are consistent with the unique radar signatures in the wake of ships. These simulations, performed to understand the short wave dampening of radar signatures behind boats, give a complementary explanation of wake behavior in addition to the surfactant measurements.

In the case of whale flukeprints, it becomes less clear whether natural ocean surfactants play a significant role. Flukeprints are

often observed in the wake of whales that have not broken the surface of the water while swimming. Without breaking the surface there may be no significant source of bubbles to initiate the harvesting of natural ocean surfactants. Testing elevated surfactant levels inside a flukeprint is a much more significant challenge than measuring in a ship wake because of possible danger to the whales and the fact that flukeprints only last several minutes (as opposed to hundreds of minutes in the case of a ship wake). We cannot entirely rule out the role surfactants may play but it is the opinion of the authors that, at best, surfactants may play a complementary role in the damping of waves inside the print, accentuation of the ridge at the edge of the print, and extension of the duration of a flukeprint after the initial breakwater effect has begun to diminish.

7. Experimental observations

To visualize the formation of vortex rings observed in numerical simulations, we conducted experiments using a thin robotic fluke. The purpose of this set of experiments was to collect qualitative rather than quantitative data. The first goal was to observe in detail the formation and the shedding of vortex rings using an artificial fluke. The second goal was to observe the surface prints created by vortex rings and the variation in surface pattern due to the angle of incidence of the ring with the surface.

We compared two motions designed to approximate that of whales: a stroke initiating at 60° from horizontal (motivated by a typical dive angle for blue whales) and a stroke oscillating from $\pm 12.5^\circ$ (motivated by the motion of whales swimming horizontally beneath the surface). While the motion of the robotic fluke in our experiments is only a rough approximation of whale motion, our observations are consistent with the theory and previous experiments described in Sections 4 and 5.

The experiments were conducted in collaboration with FloMetrics in San Diego in a tank of water approximately 122 cm long by 61 cm wide by 49 cm tall. A fluke made of slightly flexible polycarbonate of uniform (0.16 cm) thickness was patterned from the photograph of the blue whale fluke in the insert of Fig. 5, and scaled to be 0.2 m tip to tip. In comparison, blue whale flukes are 5–6 m tip to tip.

The fluke pivoted on an axis supported by an apparatus that could be adjusted to prescribe the depth of the fluke, the inclination angle and the range of motion. For each trial in the experiment, the fluke made one oscillation from the prescribed top position (with the fluke nearest the surface), down and up again. For one motion the top position with the fluke nearest the surface began at 60° from horizontal, then swept 25° down and then returned up. For the other motion the fluke began at 12.5° from horizontal, then swept 25° down and up. Both oscillations were maintained at 0.32 Hz with gearing attached to a motor. There was no forward motion of the apparatus. For comparison blue whale fluke oscillations occur at about 0.5–1.0 Hz with forward velocity 1–1.5 m/s.

To visualize the flow, we used a laser sheet generated by a 1 Watt green laser positioned to shine through a 3 mm diameter stirring rod. Plastic tubing attached along the length of the fluke (as if along the length of the tail), was connected to a syringe that was used to inject small fluorescing flakes as the fluke was oscillating. The small fluorescing particles were slightly negatively buoyant and would settle to the bottom of the tank in about 20 min. Using the two-dimensional laser sheet, we observed the generation of two three-dimensional vortex rings: one ring was shed on the downstroke and the other was shed on the upstroke. We viewed the rings from several positions one each side of the tank (using vertical sheets) and from the top (using horizontal sheets). In addition, to visualize the surface flow, we added 0.48 cm diameter buoyant polystyrene beads to the surface and observed their advection as the vortex ring interacted with the surface. An HD camera, recording 30 frames per second was positioned to record the experiments. The setup in the lab and a close-up of the fluke can be seen in Fig. 5.

Figs. 7–12 contain time series of typical experimental runs viewed from the top and from the long side of the tank for the two different initial angles. (We also made observations for runs beginning at 75°, but the results did not differ qualitatively from those beginning at 60°.) For each of the initial configurations, we conducted at least five runs. The objective of these experiments was to make qualitative observations of the dynamics of the vortex ring/surface interactions rather than quantitative measurements of flow speeds or ring evolution.

The first three sets of images are from experiments with a start position of 60° in which the fluke sweeps down and up 25°. The side views in Fig. 7 show the formation of two vortex rings, one of which moves upwards, contacts the surface head-on and spreads out horizontally, in qualitative agreement with numerical and experimental observations from the idealized vortex ring literature, as described above. The small particles are ejected through the small tube that runs along the length of the fluke, beginning in Fig. 7a at the beginning of downward sweep. The first vortex ring is forming in Fig. 7b and is released in Fig. 7c toward the side of the tank as the fluke motion reverses. The upward-moving vortex ring is forming in Fig. 7d and has made contact with the surface in Fig. 7e in which the symmetry of the left and right spreading leads to the roughly circular shape in the top views.

The top views of Figs. 8 and 9 emphasize the circular shape of the leading edge of the surface flow. The motion of the large particles in Fig. 8b–d shows the outward flow at the center is more rapid,

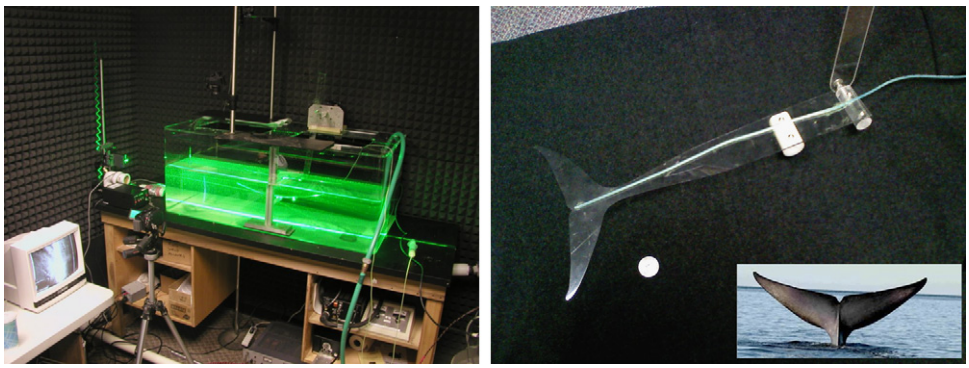

Fig. 5. Experimental setup in lab (left) for vertical laser sheet. Camera is positioned for side view. Polycarbonate fluke (right) and tubing for ejection of small particles. Quarter-size coin included for scale. Insert on right is the original photograph of the blue whale (*Balaenoptera musculus*) fluke used to pattern the experimental fluke. (Photo courtesy of Students on Ice.)

causing the inner particles to catch up with those further from the center and eventually forms a ring in Fig. 8e. As expected from the theory, Fig. 8f shows the instabilities at the edge of the ring have begun to form and surface normal vorticity has caused the particles to begin to eddy around each other. In the sequence of Fig. 9 the small particles emphasize the circular shape of the surface pattern and the instabilities forming in Fig. 9d and e.

In contrast, the experiments in which the fluke oscillates from 12.5° leads to a different surface flow pattern. In the side view of Fig. 10, the vortex ring moving upwards approaches the surface at an oblique angle. As a consequence, the two sides of the ring make contact with the surface at different times, resulting in different dynamics on each side of the ring. On the side closest to the fluke, vortex stalls (whether or not the fluke remains near the surface). The other side of the ring travels outwards, but is retarded at the place opposite the stalled vortex. Some of the particles in this retarded part of the ring can be seen in the right vortex in Fig. 10e, which is a slice slightly off-center toward the camera.

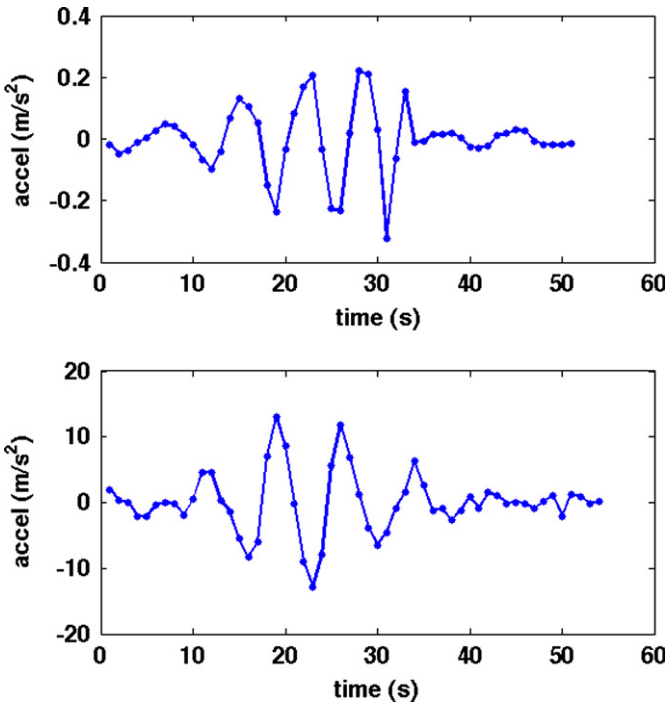

Fig. 6. Data from tags with suction cups deployed onto whales by Cascadia Research to capture fluke motion. Plots from a humpback whale (top) and a blue whale (bottom) contain typical fluking sequences. This data provided the period of the fluking oscillation but not the velocity.

In the top view of Fig. 11, the retarding of the opposite side creates a striking heart-shaped surface profile. The same heart shape can be seen in the experiment of Fig. 12, although it is more subtle due to the smaller concentration of particles in the plane of the laser sheet below the surface. Note that in the early view of Fig. 12b, the concentration of particles from the trailing side of the ring that are rising to the surface has not yet been pulled inward. In Fig. 12c, the particles have deformed and in Fig. 12d and e the characteristic shape has developed. This heart-shaped profile for oblique collisions of vortex rings with surfaces is the same phenomenon described above from the experimental work of Gharib and Weigand [33], in which they show the same pattern using a shadowgraph as in Fig. 4.

The Reynolds number can provide a measure of the difference in scale between our experiment and the motion of a whale fluke. To calculate the Reynolds number, we use the vertical tip velocity of the fluke, calculated from the vertical distance travelled in one cycle, the kinematic viscosity of fresh or seawater at 20 °C, and the measurement across the fluke tip to tip. Since our experimental fluke oscillates in a slight arc but has no significant forward component, we calculate the vertical distance travelled in one cycle. For the whale experiments, we used data collected by Calambokidis Research from tags with suction cups that track the fluke motion of whales. The swimming strokes are obtained from a high pass filter from an accelerometer attached to the whale. In theory, zero will represent the mid-line of the whale, since the tag is general parallel to the direction of travel of the whale. The data plotted in Fig. 6, contain typical patterns for a humpback whale (above) and a blue whale (below). For more information about the tagging procedures and related data, please see [37–39].

The table below contains the calculation for the Reynolds number, based on typical lengths of the caudal peduncle (tail) estimated as one-quarter of the body length, and an oscillation sweeping 30°. For kinematic viscosity we used the values of

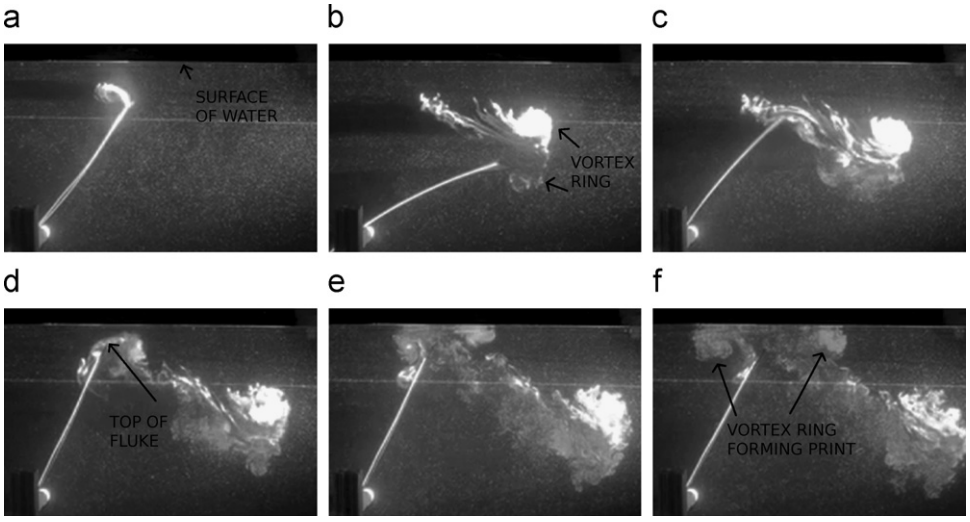

Fig. 7. Vertical laser sheet providing side view of experiment with small particles. Start angle of 60° from horizontal. Sweep down and up of 25°. (a) shows the initial ejection of small particles and beginning of downward sweep. (b) shows vortex ring forming and in (c) released toward side of tank as motion of fluke reverses. (d) shows the formation of upward-moving ring. (e) shows the symmetry of the left and right spreading rate leading to the roughly circular shape in the top views. (f) shows the breakup of the ring. (a) t=0 s; (b) t=1.43 s; (c) t=2.03 s; (d) t=2.70 s; (e) t=3.27 s and (f) t=4.00 s.

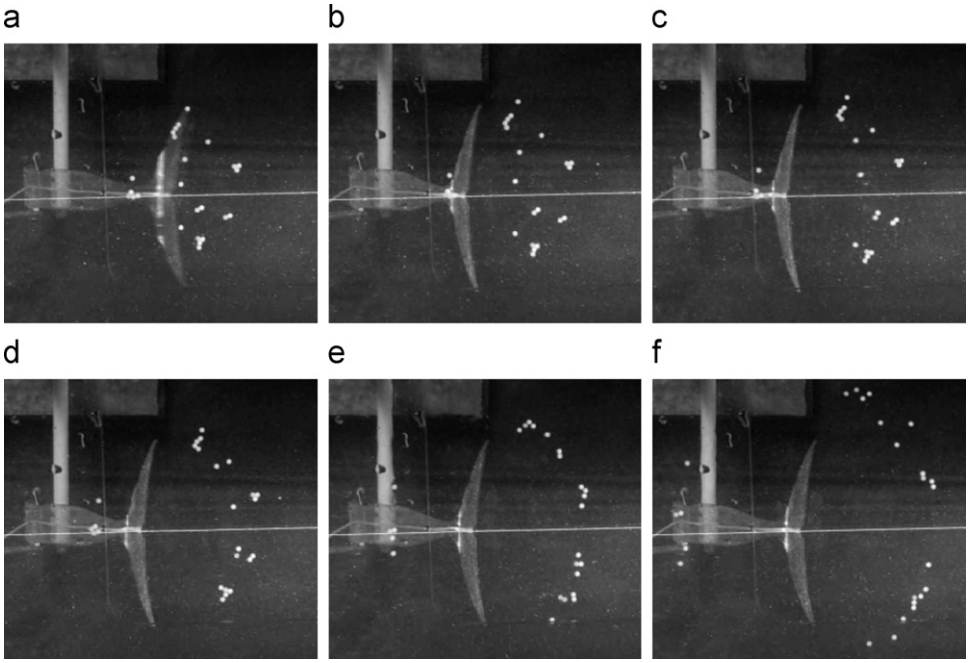

Fig. 8. Horizontal laser sheet providing top view of experiment with small particles. Start angle of 60° from horizontal. Sweep down and up of 25°. (a) is the initial position of the particles before the vortex ring has affected surface. (b–d) show rapid outward motion of particles. Surface velocity is greatest near the center of the ring, so inner particles "catch up" with outer particles. (e) shows final ring formation and (e) shows breakup of the ring. (a) t=0 s; (b) t=0.33 s; (c) t=0.63 s; (d) t=0.87 s; (e) t=1.60 s and (f) t=2.70 s.

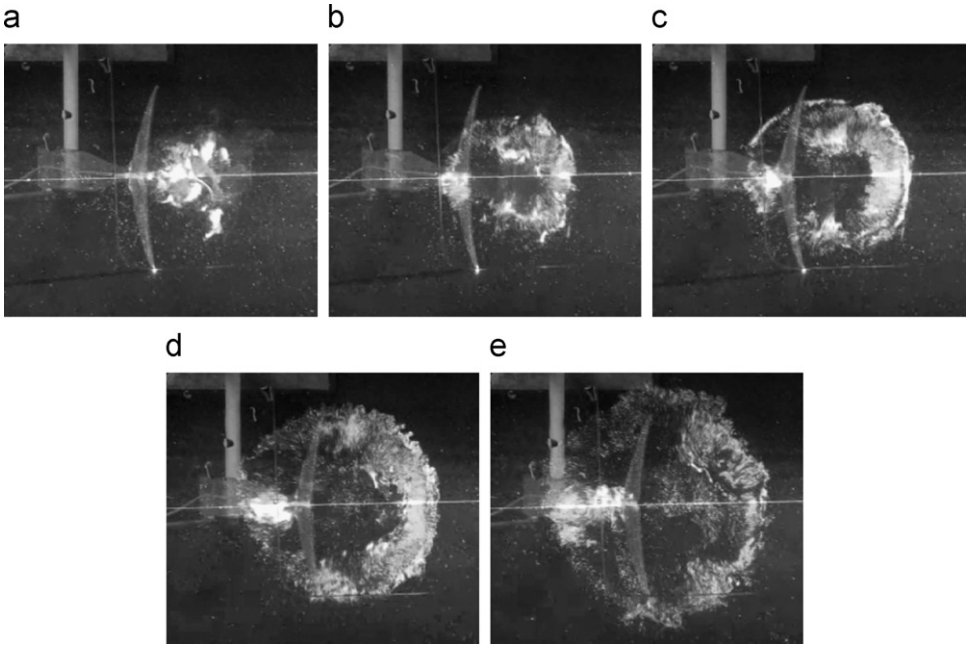

Fig. 9. Horizontal laser sheet providing top view of experiment with small particles. Start angle of 60° from horizontal. Sweep down and up of 25°. (a) and (b) show formation of vortex ring and initial ascent to surface. (c) and (d) show outward motion of particles and secondary vortices forming at outer edges. (e) shows breakup of the ring. (a) t=0 s; (b) t=0.23 s; (c) t=0.43 s; (d) t=0.70 s and (e) t=1.03 s.

freshwater for the experiment and seawater for the whales, both at 20 °C. The Reynolds number for the humpback whale, 15 m in body length and fluke 4 m wide, is estimated at 2.178×10^6 and for the blue whale, 22 m in body length and fluke 6 m wide, is estimated at 4.792×10^6. These Reynolds numbers are within typical ranges for these species. Note that in many papers on Cetaceans, the characteristic velocity in the Reynolds number is the forward velocity. This would be inappropriate for comparison to our experiments since the pivot point for our fluke oscillations was stationary. We realized that given these calculations, we would not be able to scale our motion in our lab to match that of the whales, since with our size fluke (patterned from a blue whale), we would have to achieve a vertical velocity of 240.5 m/s. Instead, we focused not on this metric (or on Strouhal number which requires a forward velocity), but on achieving a Reynolds number consistent with vortex ring formation. The experimental Reynolds number is

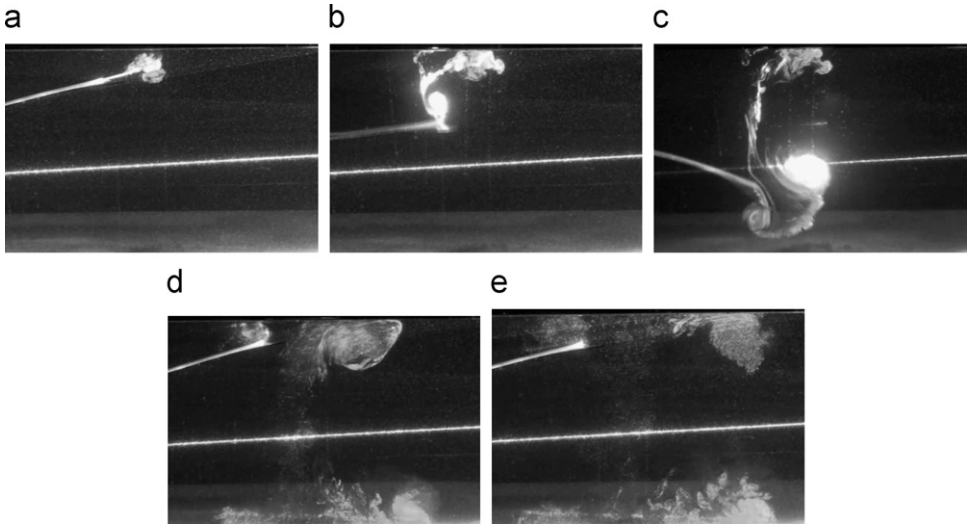

Fig. 10. Vertical laser sheet providing side view of experiment with small particles. Start angle of 12° from horizontal. Sweep down and up of 25°. (a) shows initial ejection of small particles. (b–c) show formation of downward moving ring created by downstroke and shed when the stroke reverses direction. (d–e) show clear retarding of vortex above fluke and outward motion of fluid at the other side of the ring. This retarding also occurred in experiments, where the fluke was not left at the surface. The stationary vortex retards surface velocity of fluid moving away, forming heart-shaped pattern in the top views of Figs. 12 and 11. (a) t=0 s; (b) t=1.10 s; (c) t=1.87 s; (d) t=3.60 s and (e) t=4.83 s.

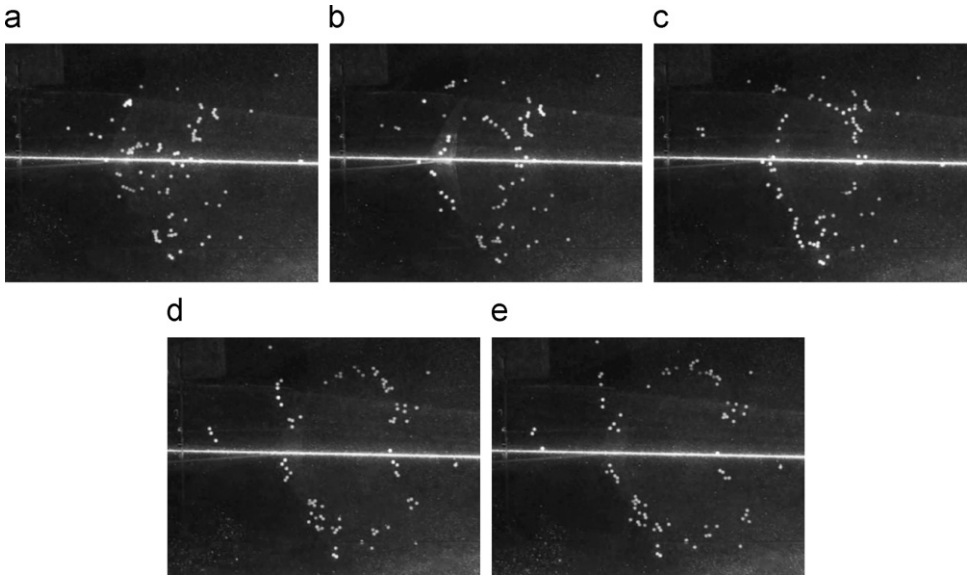

Fig. 11. Horizontal laser sheet providing top view of experiment with large particles. Start angle of 12° from horizontal. Sweep down and up of 25°. (a–e) show the surface directly above the fluke is relatively stationary as the vortex below stagnates. This rotation retards the motion on the opposite side of the ring, causing the heart-shaped surface pattern that is characteristic of oblique vortex ring-surface collisions. (a) t=0 s; (b) t=0.73 s (c) t=1.43 s; (d) t=2.97 s and (e) t=3.43 s.

calculated to be 1.67×10^3, which is large enough to be consistent with vortex ring formation (above 1000), and also on the same order as many of the numerical simulations referenced in Section 5.

	Experiment	Humpback whale	Blue whale
Vert. vel. U (m/s)	0.084	0.5546	0.8134
Fluke length L (m)	0.02	4.0	6.0
Kin. visc. v (m^2/s)	1.0040×10^{-6}	1.0185×10^{-6}	1.0185×10^{-6}
$Re = UL/v$	1.67×10^3	2.178×10^6	4.792×10^6

8. Conclusion

In this paper we have investigated the origin of whale flukeprints by integrating results from several areas of fluid dynamics: vortex shedding from flapping foils, interaction of vortex rings with surfaces, disruption of surface waves by oncoming currents, and persistence of ship wakes due to harvesting of natural ocean surfactants. Theory, observation and experimental evidence suggest that vortex rings are the primary hydrodynamic mechanism in the formation of flukeprints. The motion of the whale's fluke sheds vortex ring structures that create a powerful jet of fluid circulated up through the center of the ring. When fluid from the jet contacts the surface, an outward radial surface current induces a breakwater. This in turn damps the wind-driven capillary waves in the center of the print and causes the wave-breaking observed at its edge.

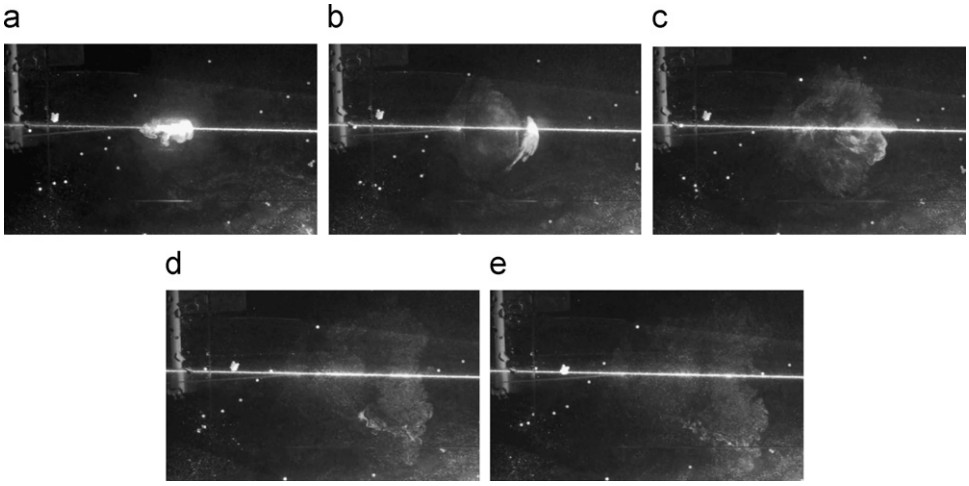

Fig. 12. Horizontal laser sheet providing top view of experiment with small particles. Start angle of 12° from horizontal. Sweep down and up of 25°. (a) shows initial ejection of particles, some of which remain on the surface in (b) as ring is moving upwards. (c–e) show development of heart-shaped pattern that results from asymmetry in the surface velocities as the vortex ring hits the surface at an oblique angle. (a) t=0 s; (b) t=2.63 s; (c) t=3.97 s; (d) t=6.63 s and (e) t=7.93 s.

We have theorized that while the primary origin of flukeprints is hydrodynamic, surfactants may play a secondary role. Despite the tendency for whales to shed in abundance, skin cells are often not observed in sufficient quantities to produce such a dramatic dampening of the short waves. In addition, the fact that whale motion does not necessarily create a large amount of white water or air bubbles compared to ship motion means the harvesting of ocean surfactants to the surface may be modest. Nonetheless, naturally occurring ocean surfactants may enhance the short wave damping as surfactants are brought up to the surface by the fluid jet.

We hope that this investigation sparks further research, to answer open questions about the formation, shape and duration of flukeprints. In the laboratory setting, there is much need for further investigation of the role of surfactants, forward velocity (using a flow tank or moving fluke), and wind generated capillary waves (perhaps created in a tank by blowing air across the surface). We hope the results of such experiments can be compared to the theoretical calculations described above. From the field, it would be valuable to have video footage of the creation of real prints from above and below the surface with an accurate time and lengthscale related to tag data recording the motion of the whale. Finally, surface tension measurements both inside and outside of a print could help provide data for comparison to results from ship wakes. Further collaboration between mathematicians, experimentalists and biologists can help answer these fundamental questions.

Acknowledgments

The work of RL was supported by ONR Grant N000141010641, HMC internal funding and the HMC Center for Environmental Studies. The work of DU was supported in part by DMS-0902792 and UC Lab Fees Research Grant 09-LR-04-116741-BERA. Any findings, conclusions, opinions, or recommendations are those of the authors, and do not necessarily reflect the views of the NSF. The authors would like to thank Michael Uminsky for the schematic drawings in Figs. 2 and 3, Prof. Gharib and J.F.M. for permission to reprint the shadowgraphs in Fig. 4, and Jeremy Goldbogen for the fluke motion data of Fig. 6.

References

[1] J. Churnside, L. Ostrovsky, T. Veenstra, Thermal footprints of whales, Oceanography 22 (2009) 109–206.
[2] J. Bush, Marangoni flows, 〈web.mit.edu/1.63/www/Lec-notes/Surfacetension/Lecture4.pdf〉.
[3] P. Pershan, The structure liquid surfaces, liquids.seas.harvard.edu/peter/presentations/Argonne6-05-12.ppt.
[4] M.M. Rubin, Intoxicating sights and smells of Hawaii flavor her reverie, Pittsburgh Post-Gaz. 30 (April) (1995) H-10.
[5] H. Huhnerfuss, Oil on troubled waters—a historical survey, in: M. Gade, G. Korenowski, H. Hühnerfuss (Eds.), Marine Surface Films, Springer-Verlag, Berlin, 2002, pp. 3–12.
[6] R.D. Peltzer, O.M. Griffin, W.R. Barger, J.A.C. Kaiser, High-resolution measurement of surface-active film redistribution in ship wakes, J. Geophys. Res. 97 (C4) (1992) 5231–5252.
[7] J.H. Milgram, R.D. Peltzer, O.M. Griffin, Suppression of short sea waves in ship wakes: measurements and observations, J. Geophys. Res. 98 (C4) (1993) 7103–7114.
[8] J.H. Milgram, R.A. Skop, R.D. Peltzer, O.M. Griffin, Modeling short sea wave energy distributions in the far wakes of ships, J. Geophys. Res. 98 (C4) (1993) 7115–7124.
[9] A.N. Baker, B. Madon, Brydei's whales (Balaenoptera cf. brydei Olsen 1913) in the Hauraki Gulf and northeastern New Zealand waters, Sci. Conserv. 272 (2007) 1–14.
[10] A.W. Lang, W.D. Thacker, On the interaction of water waves with a surface-parallel vortex, J. Fluids Eng. 130 (5) (2008) 051302.
[11] E. Valsecchi, D. Glockner-Ferrari, M. Ferrari, W. Amos, Molecular analysis of the efficiency of sloughed skin sampling in whale population genetics, Mol. Ecol. 7 (10) (1998) 1419–1422.
[12] J. Mann, R.C. Connor, P.L. Tyack, H. Whitehead, Cetacean Societies: Field Studies of Dolphins and Whales, Chicago Press, Chicago, 2000.
[13] T.V. Parshikova, Involvement of surfactants in the regulation of the development of microscopic algae, Hydrobiol. J./Gidrobiologicheskiy Zh. 39 (2003).
[14] J.T. Evans, Pneumatic and similar breakwaters, Proc. R. Soc. London A 231 (1187) (1995) 457–466.
[15] G.I. Taylor, The action of a surface current used as a breakwater, Proc. R. Soc. London A 231 (1187) (1995) 466–478.
[16] M.S. Longuet-Higgins, R.W. Stewart, The changes in amplitude of short gravity waves on steady non-uniform currents, J. Fluid Mech. 10 (04) (1961) 529–549.
[17] I. Brevik, Partial wave damping in pneumatic breakwaters, J. Hydraul. Div. 102 (9) (1976) 1167–1176.
[18] I. Borazjani, F. Sotiropoulos, Numerical investigation of the hydrodynamics of carangiform swimming in the transitional and inertial flow regimes, J. Exp. Biol. 211 (2008) 1541–1558.
[19] H. Dong, R. Mittal, F.M. Najjar, Wake topology and hydrodynamic performance of low-aspect-ratio flapping foils, J. Fluid Mech. 566 (2006) 309–343.
[20] J.D. Eldredge, Numerical simulation of the fluid dynamics of 2D rigid body motion with the vortex particle method, J. Comput. Phys. 221 (2) (2007) 626–648.
[21] A. von Loebbecke, R. Mittal, F. Fish, R. Mark, A comparison of the kinematics of the dolphin kick in humans and cetaceans, Hum. Movement Sci. 28 (2009) 99–112.
[22] A.V. Loebbecke, R. Mittal, R. Mark, J. Hahn, A computational method for analysis of underwater dolphin kick hydrodynamics in human swimming, Sports Biomech. 8 (2009) 60–77.
[23] Z.J. Wang, Vortex shedding and frequency selection in flapping flight, J. Fluid Mech. 410 (2000) 323–341.
[24] M. Lighthill, Hydromechanics of aquatic animal propulsion, Annu. Rev. Fluid Mech. 1 (1) (1969) 413–446.
[25] G. Lauder, E.G. Drucker, Forces, fishes, and fluids: hydrodynamic mechanisms of aquatic locomotion, News Physiol. Sci. 17 (2002) 235–240.

[26] E. Drucker, G.V. Lauder, Experimental hydrodynamics of fish locomotion: functional insights from wake visualization, Integr. Comp. Biol. 42 (2) (2002) 243–257.
[27] F. Fish, G. Lauder, Passive and active flow control by swimming fishes and mammals, Annu. Rev. Fluid Mech. 38 (1) (2006) 193–224.
[28] M. Song, L.P. Bernal, G. Tryggvason, Head-on collision of a large vortex ring with a free surface, Phys. Fluids A Fluid Dyn. 4 (7) (1992) 1457–1466.
[29] W. Chuijie, F. Qiang, M. Huiyang, Interactions of three-dimensional viscous axisymmetric vortex rings with a free surface, Acta Mech. Sin. 11 (3) (1995) 229–238.
[30] C. Chu, C. Wang, C. Hsieh, An experimental investigation of vortex motions near surfaces, Phys. Fluids A Fluid Dyn. 5 (3) (1993) 662–676 URL 〈http://link.aip.org/link/?PFA/5/662/1〉.
[31] A. Hirsat, W. Willmarth, Measurements of vortex pair interaction with a clean or contaminated free surface, J. Fluid Mech. 259 (1994) 25–45.
[32] S. Ohring, H.J. Lugt, Interaction of a viscous vortex pair with a free surface, J. Fluid Mech. 227 (1991) 47–70.
[33] M. Gharib, A. Weigand, Experimental studies of vortex disconnection and connection at a free surface, J. Fluid Mech. 321 (1996) 59–86.
[34] M. Song, N. Kachman, J. Kwon, L. Bernal, G. Tryggvason, Vortex ring interaction with a free surface, in: 18th Symposium on Naval Hydrodynamics, 1991, pp. 479–489.
[35] S. Fish, C. von Kerczek, Submerged vortex pair influence on ambient free surface waves, in: 18th Symposium on Naval Hydrodynamics, 1991, pp. 491–501.
[36] L. Wang, H. Ma, Interaction of vortices with a progressive surface wave, Mol. Ecol. 1(2) (1996).
[37] J.A. Goldbogen, J. Calambokidis, R.E. Shadwick, E.M. Oleson, M.A. McDonald, J.A. Hildebrand, Kinematics of foraging dives and lunge-feeding in fin whales, J. Exp. Biol. 209 (2006) 1231–1244.
[38] J.A. Goldbogen, J. Calambokidis, D.A. Croll, J.T. Harvey, K.M. Newton, E.M. Oleson, G. Schorr, R.E. Shadwick, Foraging behavior of humpback whales: kinematic and respiratory patterns suggest a high cost for a lunge, J. Exp. Biol. 211 (2008) 3712–3719.
[39] J.A. Goldbogen, J. Calambokidis, E. Oleson, J. Potvin, N.D. Pyenson, G. Schorr, R.E. Shadwick, Mechanics, hydrodynamics and energetics of blue whale lunge feeding: efficiency dependence on krill density, J. Exp. Biol. 214 (2011) 131–146.